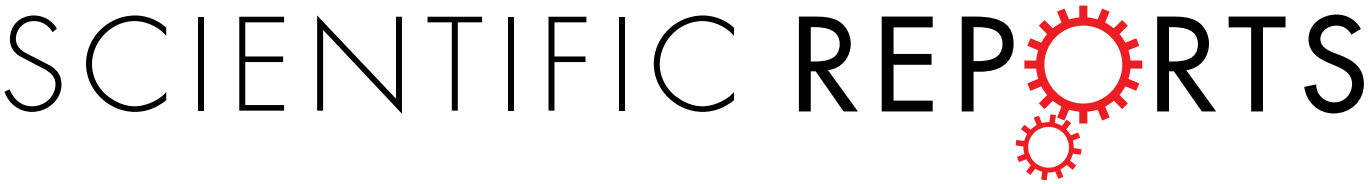

OPEN

Non-collinear magnetic structure of manganese quadruple perovskite $CdMn_7O_{12}$

Received: 13 January 2017
Accepted: 06 March 2017
Published: 05 April 2017

H. Guo[1], M. T. Fernández-Díaz[2], L. Zhou[3], Y. Yin[3], Y. Long[3,4] & A. C. Komarek[1]

We report on the magnetic structure of $CdMn_7O_{12}$ determined by powder neutron diffraction. We were able to measure the magnetic structure of this Cd containing and highly neutron absorbing material by optimizing the sample geometry and by blending the $CdMn_7O_{12}$ with Aluminum powder. Below its Néel temperature T_{N1} all magnetic reflections can be indexed by a single commensurate propagation vector $\boldsymbol{k} = (0, 0, 1)$. This is different to the case of $CaMn_7O_{12}$ where the propagation vector is incommensurate and where an in-plane helical magnetic structure has been found. We observe a commensurate non-collinear magnetic structure in $CdMn_7O_{12}$ with in-plane aligned magnetic moments resembling the ones in $CaMn_7O_{12}$. However, the commensurate propagation vector prevents the appearance of a helical magnetic structure in $CdMn_7O_{12}$. Finally, we also observe a third structural phase transition below ~60 K that can be attributed to phase separation.

The coexistence of ferroelectricity (FE) and magnetic ordering in multiferroic materials has attracted enormous attention in the past[1]. Especially the magnetoelectric coupling in these materials is of interest for possible technical applications. Multiferroics with spin induced ferroelectric properties seem to have the highest potential for sizeable magnetoelectric effects. Several possible mechanisms are able to induce FE by magnetic ordering, e.g. the inverse Dzyaloshinskii-Moriya interaction[2], the exchange striction[3] or the spin current[4] and $d-p$ hybridization effect[5,6]. The electric polarization ($\boldsymbol{P}$) in these materials is, however, usually smaller than in conventional ferroelectrics and the magnetic transition temperature not very high[7]. Hence, the observation of a comparably large $\boldsymbol{P}$ of 2870 μC/m^2 in single crystalline $CaMn_7O_{12}$ has generated intense interest in this series of manganites[8–17].

Multiferroic $CaMn_7O_{12}$[8,14] belongs to the quadruple perovskite family with general formula $(AA'_3)B_4O_{12}$. The A site is 12-fold coordinated and A' site is square-coordinated, while the B site is octahedrally coordinated. The A' site is occupied by Mn^{3+} ions and the B site by mixed valent $Mn^{3.25+}$ ions. Below ~440 K, $CaMn_7O_{12}$ undergoes a structural transition from cubic ($Im\bar{3}$) to rhombohedral ($R\bar{3}$)[18,19]. The A' ions are located at Wyckoff position 9e in space group $R\bar{3}$, and the B site Mn^{3+} and Mn^{4+} ions are located at Wyckoff positions 9d and 3b. $CaMn_7O_{12}$ undergoes two successive magnetic transitions at $T_{N1} \sim 90$ K and $T_{N2} \sim 48$ K. In the temperature range $T_{N2} < T < T_{N1}$ the magnetic structure is modulated along the c-direction with propagation vector $\boldsymbol{k} = (0, 0, 1.037)$[8]. The magnetic structure below T_{N2} becomes more complicated due to the appearance of multiple propagation vectors[17].

Except for $CaMn_7O_{12}$, the other quadruple perovskite manganites have to be synthesized under high pressure and high temperature conditions rendering the sample availability more difficult. A recent study on its analogue, $CdMn_7O_{12}$, has shown similar physical properties[11]. For example, $CdMn_7O_{12}$ also exhibits a structural transition at $T_{s1} \sim 493$ K and two successive magnetic transitions at $T_{N1} = 88$ K and $T_{N2} = 33$ K. Moreover, the magnetic transition at T_{N1} is robust against external magnetic fields, while T_{N2} can be gradually suppressed with applied magnetic field. The crystal structure of $CdMn_7O_{12}$ at room temperature is trigonal (space group $R\bar{3}$). Around $T_{s2} \sim 254$ K a commensurate structural modulation $R\bar{3} \rightarrow P\bar{3}$ has been reported recently[15].

In this paper, we report the magnetic structure of $CdMn_7O_{12}$ determined by powder neutron diffraction (PND). We focus on the temperature range $T_{N2} < T < T_{N1}$, where the magnetic peaks can be indexed by a single propagation vector like in $CaMn_7O_{12}$. However, for $CdMn_7O_{12}$ the propagation vector amounts to $\boldsymbol{k} = (0, 0, 1)$

[1]Max-Planck-Institute for Chemical Physics of Solids, Nöthnitzer Str. 40, Dresden D-01187, Germany. [2]Institut Laue-Langewin (ILL), 71 avenue des Martyrs, F-38042, Grenoble Cedex 9, France. [3]Beijing National Laboratory for Condensed Matter Physics, Institute of Physics, Chinese Academy of Sciences, P. O. Box. 603, Beijing, 100190, China. [4]Collaborative Innovation Center of Quantum Matter, Beijing, 100190, China. Correspondence and requests for materials should be addressed to Y.L. (email: ywlong@iphy.ac.cn) or A.C.K. (email: Alexander.Komarek@cpfs.mpg.de)

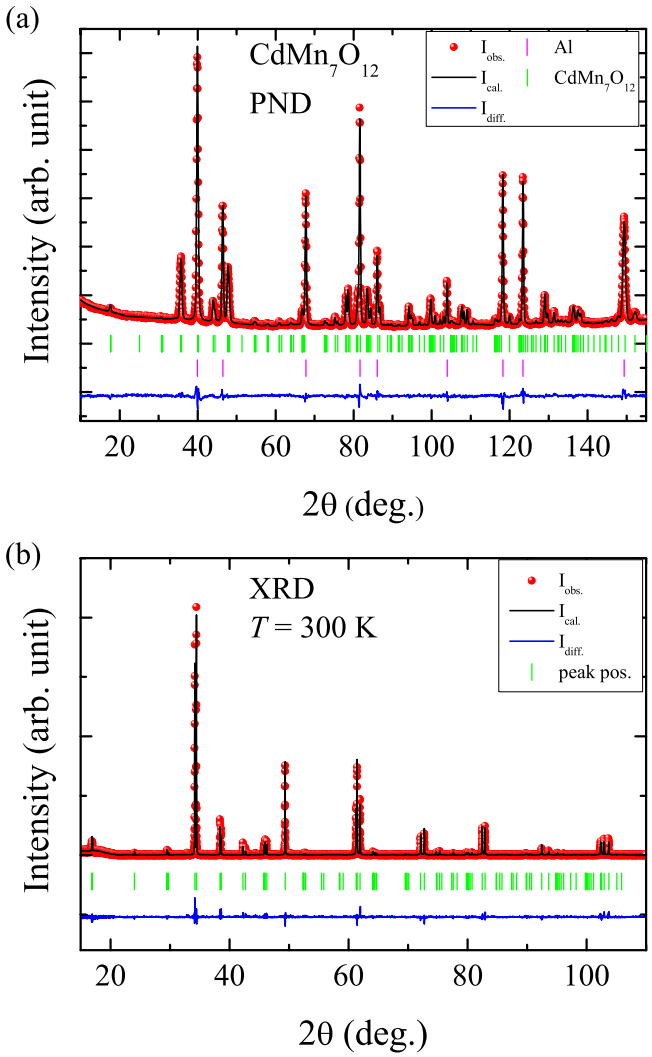

Figure 1. Rietveld fit of the room-temperature crystal structure of $CdMn_7O_{12}$ measured by (**a**) powder neutron diffraction at the D2B diffractometer with wavelength $\lambda = 1.59$ Å and (**b**) x-ray powder diffraction with wavelength $\lambda = 1.5406$ Å.

atom	x	y	z	B_{iso}
Cd1(3a)	0	0	0	1.36(18)
Mn1(9e)	1/2	0	0	0.62(5)
Mn2(9d)	1/2	0	1/2	0.62(5)
Mn3(3b)	0	0	1/2	0.62(5)
O1(18f)	0.2264(4)	0.2789(4)	0.0822(4)	1.02(2)
O2(18f)	0.3430(4)	0.5235(3)	0.3467(7)	1.02(2)

Table 1. Atomic position of $CdMn_7O_{12}$ at room-temperature obtained from Rietveld refinement of the PND pattern measured at D2B. The reliability factor is $R_{Bragg} = 8.88\%$, $\chi^2 = 2.76$. The space group is $R\bar{3}$, lattice constant $a = 10.4306(1)$ Å, $c = 6.3184(1)$ Å.

which is in contrast to $CaMn_7O_{12}$ where an incommensurate propagation vector along the *c*-direction has been observed. The magnetic structure of $CdMn_7O_{12}$ is non-collinear.

Results and Discussion

Figure 1 shows the Rietveld fit of the room temperature crystal structure measured both by PND and XRD (space group $R\bar{3}$). In Fig. 1(a), the few peaks of the Al powder did not interfere significantly with sample reflections and a reliable refinement of the crystal structure of $CdMn_7O_{12}$ could be obtained. The structural parameters are listed in Table 1. The refined volume fractions of Al and $CdMn_7O_{12}$ amount to 69.7(5)% and 30.3(2)% respectively.

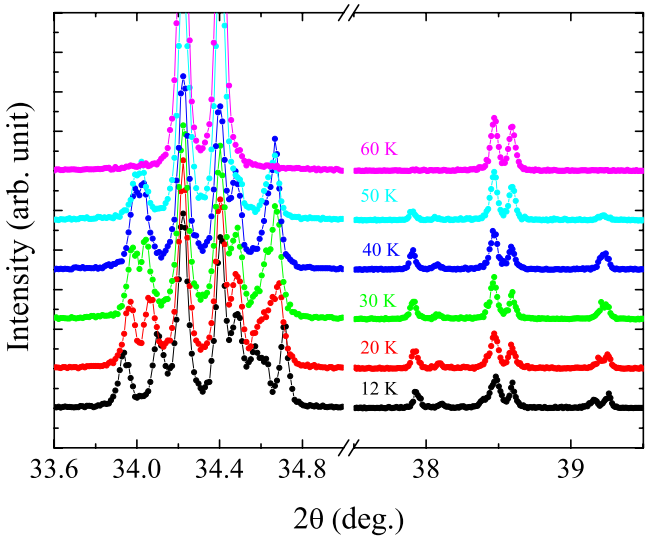

Figure 2. Temperature dependence of the XRD patterns measured at 60 K, 50 K, 40 K, 30 K, 20 K and 12 K. As can be seen, additional peaks appear below $T_{s3} \sim 60$ K. These additional peaks are indicative for phase separation and can be attributed to a second phase appearing below T_{s3}. (The patterns are shifted for clarity).

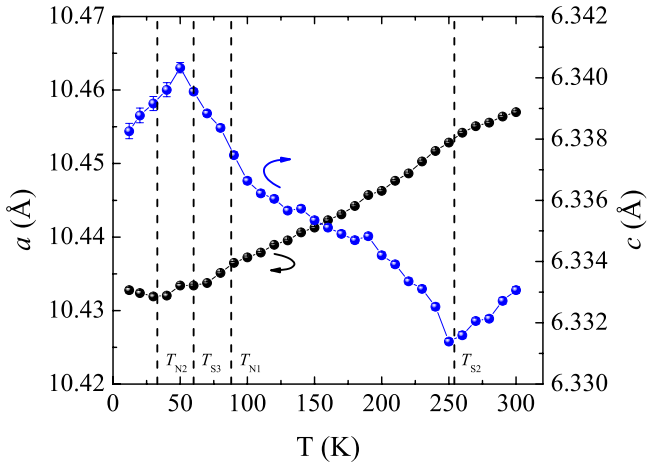

Figure 3. Temperature dependence of the lattice constant (space groups $P\bar{3}$ and $R\bar{3}$) determined by x-ray powder diffraction.

Note, that indications for a structural transition $R\bar{3} \rightarrow P\bar{3}$ at $T_{s2} \sim 254$ K have been reported recently[15].

We performed temperature dependant powder X-ray diffraction experiments down to 12 K and were able to observe an additional structural transition at $T_{s3} \sim 60$ K. Note, that there is a small anomaly at ~60 K in specific heat measurements at high magnetic fields of 9 T, whereas no obvious anomaly could be observed in zero field measurements[11]. Our measurements are indicative for the occurrence of phase separation below T_{s3} similar as observed in other transition metal oxides like $SrCrO_3$[20]. Below T_{s3}, the intensity of the main peaks related to the $P\bar{3}$ phase decreases and additional peaks appear which belong to a lower symmetry phase, see Fig. 2. This would be consistent with a scenario where phase separation occurs below T_{s3} and where only a certain volume fraction of the compound undergoes the structural transition (that might be enhanced by applying magnetic fields of 9 T). The origin of this structural transition requires further studies. Here, we focus mainly on the magnetic structure determination of $CdMn_7O_{12}$ slightly above or around T_{s3}.

We determined the lattice parameters of the $R\bar{3}$ and $P\bar{3}$ phases in the entire measured temperature range, see Fig. 3. The lattice parameters show an anisotropic thermal expansion. The *a* lattice constant decreases continuously with decreasing temperature until T_{N2}. A small kink can be observed at T_{s2} while no obvious anomaly can be found at T_{N1}. Then, below T_{N2}, *a* starts to increase with decreasing temperature. On the other hand, the *c* lattice constant exhibits distinct anomalies at T_{s2} and also at 100 K and 50 K. This behaviour is similar to the one in $CaMn_7O_{12}$[21]. The temperatures of 100 K and 50 K are somewhat higher than the magnetic transition temperatures T_{N1} and T_{N2}, suggesting that the magnetic transitions follow the structural ones.

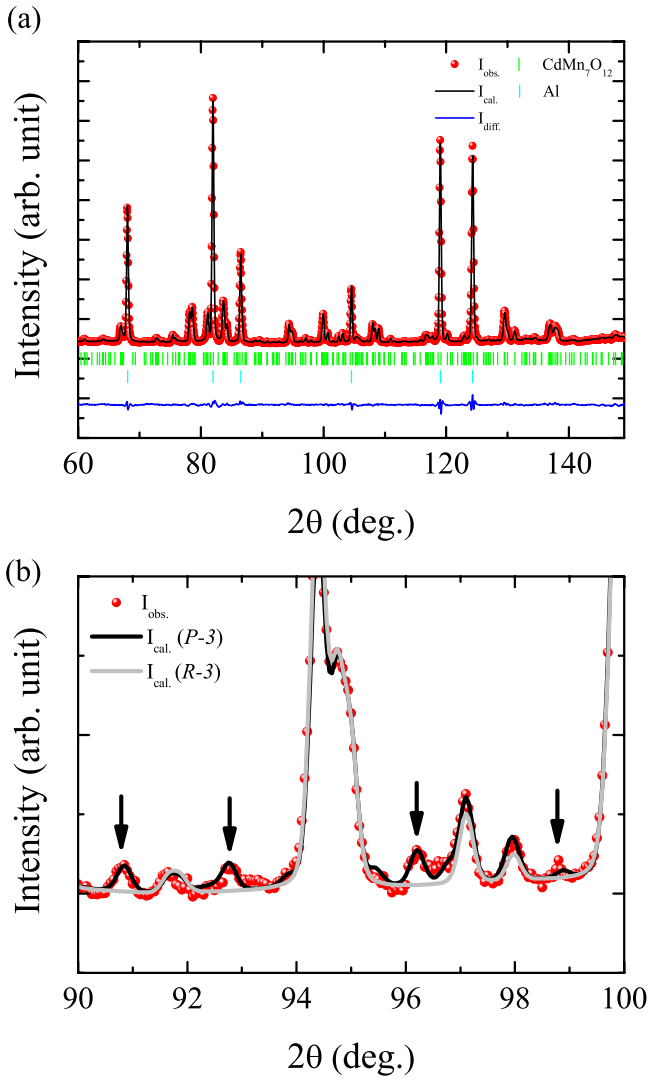

Figure 4. Rietveld fit of the powder neutron diffraction patterns measured at D2B diffractometer with wavelength $\lambda = 1.59$ Å at 40 K. (**a**) The nuclear structure is refined in the high 2θ range with space group $P\bar{3}$. (**b**) Comparison of the pattern refined by using the space group $R\bar{3}$ and $P\bar{3}$. Arrows indicate the peaks which cannot be described by the space group $R\bar{3}$.

We studied the crystal structure of $CdMn_7O_{12}$ at 40 K by means of powder neutron diffraction at the D2B diffractometer. The peak-splitting that has been observed in our high-resolution XRD measurements could not be resolved in our neutron measurements with less resolution. In Fig. 4(a) a refinement of the crystal structure with one single phase (space group $P\bar{3}$) is shown. For comparison, the pattern refined with space group $R\bar{3}$ is also shown in Fig. 4(b). The additional peaks indicated by the arrows cannot be described by space group $R\bar{3}$. The structural parameters are listed in Table 2.

We next focus on the magnetic structure refinement. We have measured the magnetic structure of $CdMn_7O_{12}$ between 2 K and 120 K at the D1B diffractometer using an incident neutron wavelength of 2.52 Å. Only two peaks from the Aluminum powder appear in the entire diffraction pattern. Thus, the dilution with fine Aluminum powder does not cause any interference with magnetic reflections that appear below the Néel temperature of $CdMn_7O_{12}$. As can be seen in Fig. 5 all peaks that appear at low temperature and that can not be indexed with space group $R\bar{3}$ vanish at the Néel temperature of $CdMn_7O_{12}$. Hence, these reflections are magnetic in origin and can not be connected to the structural transition that takes place at 254 K. For $T_{N2} < T < T_{N1}$ all magnetic peaks can be indexed with a single propagation vector $\boldsymbol{k} = (0, 0, 1)$, which is different from the incommensurate case in $CaMn_7O_{12}$. Below T_{N2} the magnetic structure is more complicated and multiple propagation vectors are necessary for describing the magnetic structure. Here, we will focus on the magnetic structure for $T_{N2} < T < T_{N1}$ only. Due to the structural transition from $R\bar{3}$ to $P\bar{3}$, the three Mn sites split into six different sites below about 200 K. Instead of a refinement with that many independent magnetic moments and moment sizes we were also able to describe the magnetic neutron scattering intensities properly in a refinement based on irreducible representations for the high symmetry crystal structure $R\bar{3}$ which is similar to a refinement in $P\bar{3}$ with certain constraints to the moments. Since the structural distortions below the structural phase transition $R\bar{3} \rightarrow P\bar{3}$ are negligible for the magnetic

atom	x	y	z	B_{iso}
Cd1(1a)	0	0	0	0.27(14)
Cd2(2d)	0.3333	0.6667	0.6784(38)	0.27(14)
Mn1(3e)	1/2	0	0	0.20(6)
Mn2(3f)	1/2	0	1/2	0.20(6)
Mn3(1b)	0	0	1/2	0.20(6)
Mn4(2d)	0.3333	0.6667	0.1471(29)	0.20(6)
Mn5(6g)	0.3357(17)	0.1608(16)	0.6529(21)	0.20(6)
Mn6(6g)	0.1653(15)	0.8216(16)	0.8333(24)	0.20(6)
O1(6g)	0.2366(17)	0.1608(16)	0.6529(16)	0.92(3)
O2(6g)	0.3486(14)	0.5223(16)	0.3486(20)	0.92(3)
O3(6g)	0.0687(10)	0.6148(14)	0.7536(20)	0.92(3)
O4(6g)	0.2815(16)	0.8988(13)	0.5815(23)	0.92(3)
O5(6g)	0.3192(16)	0.8098(15)	1.0006(18)	0.92(3)
O6(6g)	0.1461(14)	0.1458(13)	0.6914(17)	0.92(3)

Table 2. Atomic positions of $CdMn_7O_{12}$ at 40 K as obtained from Rietveld refinement of the PND pattern measured at the D2B diffractometer. The reliability factor amounts to $R_{Bragg} = 7.49\%$ with $\chi^2 = 8.66$. We used one single phase with space group $P\bar{3}$. The lattice constants amount to $a = 10.4064(1)$ Å, $c = 6.3250(1)$ Å.

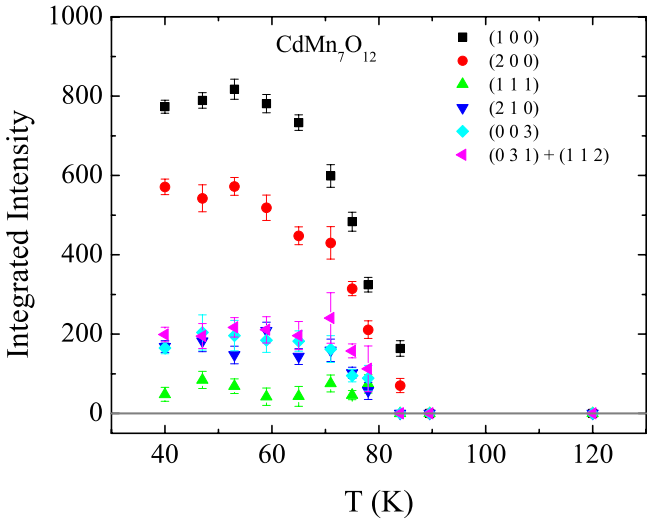

Figure 5. Temperature dependence of magnetic peaks observed in our PND patterns ($\lambda = 2.52$ Å).

structure these constraints appear reasonable. Figure 6 shows the results of our refinements for temperatures of (a) 75 K and (b) 40 K.

The magnetic reducible representation Γ of site 9*e* and 9*d* is decomposed into three irreducible representations (IRs) with dimension one, as

$$\Gamma = 3\Gamma_1 \oplus 3\Gamma_2 \oplus 3\Gamma_3. \quad (1)$$

For site 3*b*, it is also decomposed into three IR with dimension one, as

$$\Gamma = \Gamma_1 \oplus \Gamma_2 \oplus \Gamma_3. \quad (2)$$

The basis vectors (ψ_i) of the IRs are listed in Tables 3 and 4 for the 3*b* and for the 9*e*(9*d*) site respectively.

Since there are three different Mn sites in the unit cell, magnetic couplings between Mn ions at different sites require the Mn ions order according to the same IR in the first order approximation[22]. From Table 3, it can be seen that the IR Γ_1 constrains the magnetic moments at site 3*b* along the *c*-direction, while for IR Γ_2 and Γ_3, the real and imaginary components are perpendicular to each other with the same length, thus, giving rise to a non-collinear magnetic structure with moments that have the same size and that are aligned within the *ab* plane. Earlier PND studies on $CaMn_7O_{12}$ suggested a ferrimagnetic ordering with magnetic moments along the *c*-axis[23]. However, the observation of the (0 0 2) peak at $2\Theta \sim 47°$ is not indicative for this scenario based on IR Γ_1. Also if *ab* components of Mn ions at 9*e* and 9*d* sites are included for the refinement based on IR Γ_1 no satisfactory description of the measured data could be obtained. Since $CdMn_7O_{12}$ is a quite localized system, we also assume

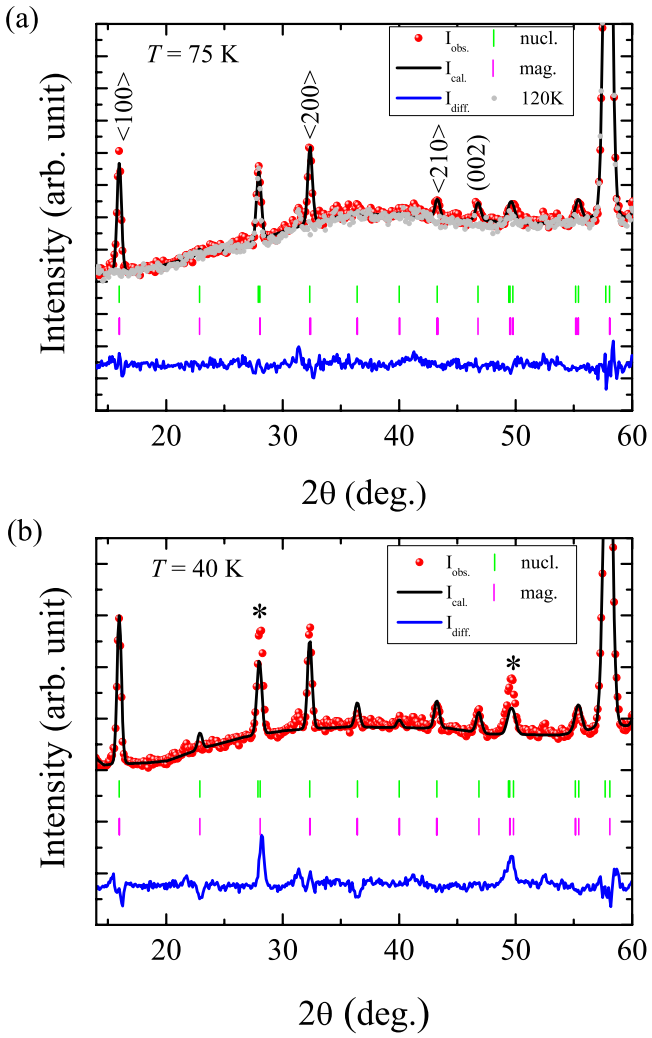

Figure 6. Rietveld refinement of the magnetic structure measured at the D1B diffractometer ($\lambda = 2.52$ Å). The magnetic structure at (**a**) 75 K (above T_{s3}) and (**b**) 40 K (below T_{s3}) can be described both by the IR Γ_3. In (**a**), additionally, the 120 K data is shown as a reference. In (**b**) the two asterisks mark the nuclear peak positions that become broader and stronger due to the structural transition below T_{s3}. However, the overall magnetic peak intensities can be still described by IR Γ_3.

Mn3 (3*b*)			$\left(0, 0, \frac{1}{2}\right)$
Γ_1	ψ_1	Re	(0, 0, 1)
Γ_2	ψ_1	Re	$\left(\frac{3}{2}, 0, 0\right)$
		Im	$\left(-\frac{\sqrt{3}}{2}, -\sqrt{3}, 0\right)$
Γ_3	ψ_1	Re	$\left(\frac{3}{2}\,0\,0\right)$
		Im	$\left(\frac{\sqrt{3}}{2}, \sqrt{3}, 0\right)$

Table 3. Basis vectors of the irreducible representations of the space group R$\bar{3}$ for sites 3*b* with propagation vector $k = (0, 0, 1)$.

no modulations of the ordered moment sizes for the 9*e* and 9*d* sites. This can be realized by a linear combination of the basis vectors as follows:

$$\psi = \left(1 + \frac{i}{\sqrt{3}}\right)\psi_1 + \frac{2i}{\sqrt{3}}\psi_2 \tag{3}$$

Mn1 (9*e*)			$\left(\frac{1}{2}, 0, 0\right)$	$\left(0, \frac{1}{2}, 0\right)$	$\left(\frac{1}{2}, \frac{1}{2}, 0\right)$
Mn2 (9*d*)			$\left(\frac{1}{2}, \frac{1}{2}, \frac{1}{2}\right)$	$\left(\frac{1}{2}, 0, \frac{1}{2}\right)$	$\left(0, \frac{1}{2}, \frac{1}{2}\right)$
Γ_1	ψ_1	Re	(1, 0, 0)	(0, 1, 0)	(−1, −1, 0)
	ψ_2	Re	(0, 1, 0)	(−1, −1, 0)	(1, 0, 0)
	ψ_3	Re	(0, 0, 1)	(0, 0, 1)	(0, 0, 1)
Γ_2	ψ_1	Re	(1, 0, 0)	$\left(0, -\frac{1}{2}, 0\right)$	$\left(\frac{1}{2}, \frac{1}{2}, 0\right)$
		Im	(0, 0, 0)	$\left(0, -\frac{\sqrt{3}}{2}, 0\right)$	$\left(-\frac{\sqrt{3}}{2}, -\frac{\sqrt{3}}{2}, 0\right)$
	ψ_2	Re	(0, 1, 0)	$\left(\frac{1}{2}, \frac{1}{2}\, 0\right)$	$\left(-\frac{1}{2}\, 0\, 0\right)$
		Im	(0, 0, 0)	$\left(\frac{\sqrt{3}}{2}, \frac{\sqrt{3}}{2}, 0\right)$	$\left(\frac{\sqrt{3}}{2}, 0, 0\right)$
	ψ_3	Re	(0, 0, 1)	$\left(0, 0, -\frac{1}{2}\right)$	$\left(0, 0, -\frac{1}{2}\right)$
		Im	(0, 0, 0)	$\left(0, 0, -\frac{\sqrt{3}}{2}\right)$	$\left(0, 0, \frac{\sqrt{3}}{2}\right)$
Γ_3	ψ_1	Re	(1, 0, 0)	$\left(0, -\frac{1}{2}, 0\right)$	$\left(\frac{1}{2}, \frac{1}{2}, 0\right)$
		Im	(0, 0, 0)	$\left(0, \frac{\sqrt{3}}{2}, 0\right)$	$\left(\frac{\sqrt{3}}{2}, \frac{\sqrt{3}}{2}, 0\right)$
	ψ_2	Re	(0, 1, 0)	$\left(\frac{1}{2}, \frac{1}{2}, 0\right)$	$\left(-\frac{1}{2}, 0, 0\right)$
		Im	(0, 0, 0)	$\left(-\frac{\sqrt{3}}{2}, -\frac{\sqrt{3}}{2}, 0\right)$	$\left(-\frac{\sqrt{3}}{2}, 0, 0\right)$
	ψ_3	Re	(0, 0, 1)	$\left(0, 0, -\frac{1}{2}\right)$	$\left(0, 0, -\frac{1}{2}\right)$
		Im	(0, 0, 0)	$\left(0, 0, \frac{\sqrt{3}}{2}\right)$	$\left(0, 0, -\frac{\sqrt{3}}{2}\right)$

Table 4. Basis vectors of the irreducible representations of the space group $R\bar{3}$ for sites 9*e* and 9*d* with propagation vector $k = (0, 0, 1)$.

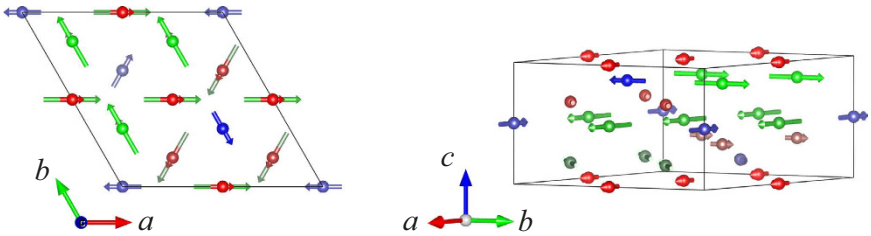

Figure 7. Magnetic structure of $CdMn_7O_{12}$ ($T_{N2} < T < T_{N1}$) projected along the *c*-direction. The red, green and blue arrows represent the magnetic moment of Mn1, Mn2 and Mn3 at the crystallographic 9*e*, 9*d* and 3*b* sites respectively. The light and dark color represent Mn ions in different layers along the *c*-direction.

Thus, the IR Γ_2 gives rise to a 120°-type noncollinear structure, while the magnetic moments are parallel to each other within the same layer for Γ_3. The former will lead to the extinction of the $(0\ 0\ l + k_z)$ reflection, which is not in agreement with our experimental observations (Fig. 6(a)). For these reasons the magnetic structure of $CdMn_7O_{12}$ can be described by the IR Γ_3. The refinable parameters are the amplitudes of the moments at three sites and the phases between them. In our refinements the phase difference between Mn1/Mn2 and Mn3 turned out to be always close to π. Therefore, we fixed the phase to this value and only the amplitude of the moments was, finally, refined. The best refinement is shown in Fig. 6(a). As can be seen, all magnetic reflections can be described in a satisfactory manner; the magnetic *R* factor amounts to 22.5%. The magnetic structure is plotted in Fig. 7. Within the same sublattice the moments are parallel to each other within the same layer (same value of *z*) and rotate by $2\pi/3$ and $4\pi/3$ when going from one layer to the next according to the centering translations (2/3, 1/3, 1/3) and (1/3, 2/3, 2/3) respectively. The net moment in the unit cell is zero, which is consistent with the magnetization measurements between T_{N1} and T_{N2}, showing linear curve of *M* vs. *H*. The magnetic structure resembles the one of $CaMn_7O_{12}$[8,24]. However, the magnetic structure of $CaMn_7O_{12}$ is incommensurate whereas the propagation vector is commensurate in the case of $CdMn_7O_{12}$.

The temperature dependence of the ordered magnetic moments for the distinct Mn sites is shown in Fig. 8. Below *TN*1, the ordered moment size starts to increase. Then, at T_{s3}, the moments at the Mn1 site exhibit an anomalous decrease whereas the Mn2 and Mn3 sites continue their increase. Note, that the size of the magnetic moments of Mn^{3+} ions at the 9*e* (Mn1) and 9*d* (Mn2) sites (the 9*e* site is square coordinated, while the 9*d* site is octahedrally coordinated by O ions) is very similar for $CaMn_7O_{12}$ which is in contrast to the case of $CdMn_7O_{12}$.

In summary, the magnetic structure of $CdMn_7O_{12}$ below its Néel temperature has been determined by PND. We observe a non-collinear magnetic structure with Mn spins that are aligned within the *ab* plane. The magnetic

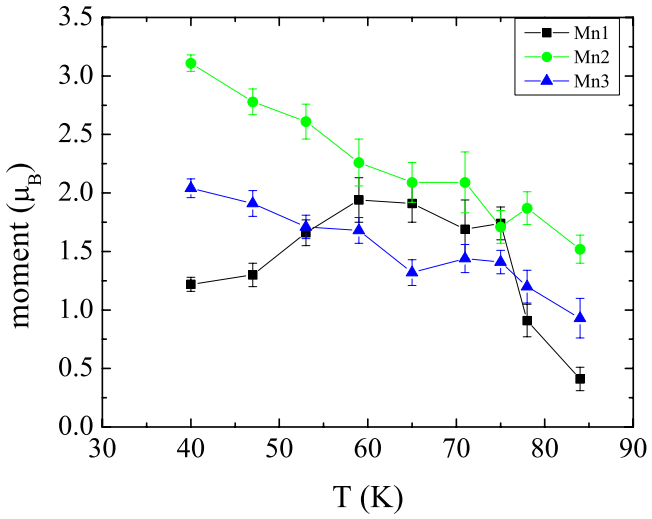

Figure 8. Temperature dependence of the magnetic moments for the distinct Mn sites.

propagation vector is commensurate with $\boldsymbol{k} = (0, 0, 1)$ which prevents the occurrence of a helical structure. This is different to the case of $CaMn_7O_{12}$.

Methods

Polycrystalline samples of $CdMn_7O_{12}$ were synthesized by high pressure method as described elsewhere[11].

Powder neutron diffraction (PND) measurements were performed at the D1B and D2B diffractometers at the Institut Laue-Langevin (ILL), France with a neutron wave length λ of 2.52 Å and 1.59 Å respectively. In order to reduce the absorption of neutrons by Cd nuclei, the $CdMn_7O_{12}$ powder was mixed with larger amount of Al powder and filled into the outer space of a hollow vanadium cylinder. This technique that we initially developed for $SmFeO_3$[25] enabled us to obtain excellent and fully evaluable neutron data of this highly neutron absorbing material (irrespective of the chosen neutron wavelength ~2.5 Å or ~1.6 Å). The PND patterns were analyzed by the Rietveld method using the Fullprof software.

In addition, temperature dependent x-ray diffraction (XRD) measurements were also performed on a Bruker D8 Discover A25 diffractometer using Cu K_{α_1} radiation. A closed cycle helium cryostat (*Phenix* of *Oxford Cryosystems*) was used for cooling the flat plate powder sample.

References

1. Zhao, L., Fernández-Díaz, M. T., Tjeng, L. H. & Komarek, A. C. Oxyhalides: A new class of high-T_c multiferroic materials. *Science Advances* **2,** e1600353 (2016).
2. Sergienko, I. A. & Dagotto, E. Role of the Dzyaloshinskii-Moriya interaction in multiferroic perovskites. *Phys. Rev. B* **73,** 094434 (2006).
3. Lu, X. Z., Whangbo, M. H., Dong, S., Gong, X. G. & Xiang, H. J. Giant ferroelectric polarization of $CaMn_7O_{12}$ induced by a combined effect of Dzyaloshinskii-Moriya interaction and exchange striction. *Phys. Rev. Lett.* **108,** 187204 (2012).
4. Katsura, H., Nagaosa, N. & Balatsky, A. V. Spin current and magnetoelectric effect in noncollinear magnets. *Phys. Rev. Lett.* **95,** 057205 (2005).
5. Arima, T.-h. Ferroelectricity induced by proper-screw type magnetic order. *J. Phys. Soc. Jpn.* **76,** 073702 (2007).
6. Nakajima, T. *et al.* Identification of microscopic spin-polarization coupling in the ferroelectric phase of magnetoelectric multiferroic $CuFe_{1-x}Al_xO_2$. *Phys. Rev. B* **78,** 024106 (2008).
7. Zhao, L. *et al.* Mn_3TeO_6 – a new multiferroic material with two magnetic substructures. *physica status solidi (RRL) – Rapid Research Letters* **9,** 730–734 (2015).
8. Johnson, R. D. *et al.* Giant improper ferroelectricity in the ferroaxial magnet $CaMn_7O_{12}$. *Phys. Rev. Lett.* **108,** 067201 (2012).
9. Sławiński, W., Przeniosło, R., Sosnowska, I. & Chrobak, A. Beats in the magnetic modulation of multiferroic $CaMn_7O_{12}$. *J. Phys. Soc. Jpn.* **81,** 094708 (2012).
10. Wang, X. *et al.* Observation of magnetoelectric multiferroicity in a cubic perovskite system: $LaMn_3Cr_4O_{12}$. *Phys. Rev. Lett.* **115,** 087601 (2015).
11. Glazkova, Y. S. *et al.* High-pressure synthesis, crystal structures, and properties of $CdMn_7O_{12}$ and $SrMn_7O_{12}$ perovskites. *Inorg. Chem.* **54,** 9081–9091 (2015).
12. Locherer, T., Dinnebier, R., Kremer, R. K., Greenblatt, M. & Jansen, M. Synthesis and properties of a new quadruple perovskite: A-site ordered $PbMn_3Mn_4O_{12}$. *J. Solid State Chem.* **190,** 277–284 (2012).
13. Perks, N. J., Johnson, R. D., Martin, C., Chapon, L. C. & Radaelli, P. G. Magneto-orbital helices as a route to coupling magnetism and ferroelectricity in multiferroic $CaMn_7O_{12}$. *Nat. Commun.* **3,** 1277 (2012).
14. Zhang, G. *et al.* Multiferroic properties of $CaMn_7O_{12}$. *Phys. Rev. B* **84,** 174413 (2011).
15. Belik, A. A. *et al.* Low-temperature structural modulations in $CdMn_7O_{12}$, $CaMn_7O_{12}$, $SrMn_7O_{12}$, and $PbMn_7O_{12}$ perovskites studied by synchrotron x-ray powder diffraction and mössbauer spectroscopy. *J. Phys. Chem. C* **120,** 8278–8288 (2016).
16. Terada, N., Glazkova, Y. S. & Belik, A. A. Differentiation between ferroelectricity and thermally stimulated current in pyrocurrent measurements of multiferroic MMn_7O_{12} (M = Ca, Sr, Cd, Pb). *Phys. Rev. B* **93,** 155127 (2016).
17. Johnson, R. D. *et al.* Modulated spin helicity stabilized by incommensurate orbital density waves in a quadruple perovskite manganite. *Phys. Rev. B* **93,** 180403 (2016).
18. Bochu, B. *et al.* Bond lengths in '$CaMn_3$'$(Mn_4)O_{12}$: A new Jahn-Teller distortion of Mn^{3+} octahedra. *Solid State Comm.* **36,** 133–138 (1980).

19. Przenioslo, R., Sosnowska, I., Suard, E., Hewat, A. & Fitch, A. N. Phase coexistence in the charge ordering transition in $CaMn_7O_{12}$. *J. Phys.: Condens. Matter* **14,** 5747 (2002).
20. Komarek, A. C. *et al.* Magnetic order, transport and infrared optical properties in the $ACrO_3$ system (A = Ca, Sr, and Pb). *Phys. Rev. B* **84,** 125114 (2011).
21. Przeniosło, R., Sosnowska, I., Suard, E., Hewat, A. & Fitch, A. N. Charge ordering and anisotropic thermal expansion of the manganese perovskite $CaMn_7O_{12}$. *Physica B: Condens. Matter* **344,** 358–367 (2004).
22. Bertaut, E. Representation analysis of magnetic structures. *Acta Cryst.* **A24,** 217–231 (1968).
23. Przeniosło, R., Sosnowska, I., Hohlwein, D., Hauß, T. & Troyanchuk, I. O. Magnetic ordering in the manganese perovskite $CaMn_7O_{12}$. *Solid State Comm.* **111,** 687–692 (1999).
24. Sławiński, W., Przeniosło, R., Sosnowska, I. & Petříček, V. Helical screw type magnetic structure of the multiferroic $CaMn_7O_{12}$ with low Cu-doping. *Acta Cryst.* **B68,** 240–249 (2012).
25. Kuo, C.-Y. *et al.* $k = 0$ magnetic structure and absence of ferroelectricity in $SmFeO_3$. *Phys. Rev. Lett.* **113,** 217203 (2014).

Acknowledgements

We thank L. Zhao and L. H. Tjeng for fruitful discussions. Y. Long was supported by 973 Project of the Ministry of Science and Technology of China (Grant No. 2014CB921500), the Strategic Priority Research Program of the Chinese Academy of Sciences (Grant No. XDB07030300), and the National Natural Science Foundation of China (Grant No. 11574378).

Author Contributions

Conceiving experiments and project management: A.C.K.; conducting and analyzing experiments: H.G., M.T.F. and A.C.K.; synthesizing samples: L.Z., Y.Y. and Y.L.; manuscript writing: H.G. and A.C.K.

Additional Information

Competing Interests: The authors declare no competing financial interests.

How to cite this article: Guo, H. *et al.* Non-collinear magnetic structure of manganese quadruple perovskite $CdMn_7O_{12}$. *Sci. Rep.* **7**, 45939; doi: 10.1038/srep45939 (2017).

Publisher's note: Springer Nature remains neutral with regard to jurisdictional claims in published maps and institutional affiliations.

This work is licensed under a Creative Commons Attribution 4.0 International License. The images or other third party material in this article are included in the article's Creative Commons license, unless indicated otherwise in the credit line; if the material is not included under the Creative Commons license, users will need to obtain permission from the license holder to reproduce the material. To view a copy of this license, visit http://creativecommons.org/licenses/by/4.0/

© The Author(s) 2017

SCIENTIFIC REPORTS

OPEN

Corrigendum: Non-collinear magnetic structure of manganese quadruple perovskite $CdMn_7O_{12}$

H. Guo, M. T. Fernández-Díaz, L. Zhou, Y. Yin, Y. Long & A. C. Komarek

Scientific Reports 7:45939; doi: 10.1038/srep45939; published online 05 April 2017; updated on 04 May 2017

The original version of this Article contained an error in the spelling of the author M. T. Fernández-Díaz, which was incorrectly given as M. T. Fernández-Daz. This error has now been corrected in the PDF and HTML versions of the Article.

This work is licensed under a Creative Commons Attribution 4.0 International License. The images or other third party material in this article are included in the article's Creative Commons license, unless indicated otherwise in the credit line; if the material is not included under the Creative Commons license, users will need to obtain permission from the license holder to reproduce the material. To view a copy of this license, visit http://creativecommons.org/licenses/by/4.0/

© The Author(s) 2017